Experimental investigation of the equilibrium and stability of long towed cable systems

Martin Obligado, Mickaël Bourgoin

▶ **To cite this version:**

Martin Obligado, Mickaël Bourgoin. Experimental investigation of the equilibrium and stability of long towed cable systems. New Journal of Physics, 2013, 15, pp.043019. 10.1088/1367-2630/15/4/043019 . hal-00941506

HAL Id: hal-00941506
https://hal.science/hal-00941506

Submitted on 27 May 2020

HAL is a multi-disciplinary open access archive for the deposit and dissemination of scientific research documents, whether they are published or not. The documents may come from teaching and research institutions in France or abroad, or from public or private research centers.

L'archive ouverte pluridisciplinaire **HAL**, est destinée au dépôt et à la diffusion de documents scientifiques de niveau recherche, publiés ou non, émanant des établissements d'enseignement et de recherche français ou étrangers, des laboratoires publics ou privés.

Distributed under a Creative Commons Attribution - ShareAlike 4.0 International License

IOPscience iopscience.iop.org

Home Search Collections Journals About Contact us My IOPscience

An experimental investigation of the equilibrium and stability of long towed cable systems

This article has been downloaded from IOPscience. Please scroll down to see the full text article.

2013 New J. Phys. 15 043019

(http://iopscience.iop.org/1367-2630/15/4/043019)

View the table of contents for this issue, or go to the journal homepage for more

Download details:
IP Address: 195.220.27.56
The article was downloaded on 25/04/2013 at 14:38

Please note that terms and conditions apply.

New Journal of Physics
The open access journal for physics

An experimental investigation of the equilibrium and stability of long towed cable systems

Martin Obligado and Mickaël Bourgoin[1]
Laboratoire des Écoulements Géophysiques et Industriels, CNRS/UJF/G-INP UMR 5519, BP53, F-38041 Grenoble, France
E-mail: mickael.bourgoin@legi.grenoble-inp.fr

New Journal of Physics **15** (2013) 043019 (22pp)
Received 19 September 2012
Published 15 April 2013
Online at http://www.njp.org/
doi:10.1088/1367-2630/15/4/043019

Abstract. The dynamics of towed objects in a fluid environment is of interest for many practical situations. We investigate experimentally the equilibrium and stability of the trajectory of a sphere towed at constant velocity at the tip of a cable with an unprecedented large length-to-diameter aspect ratio, exceeding 10^4. The towing configuration is artificially obtained by considering a steady cable (with one fixed end and a free end to which a sphere is eventually attached) in a low-turbulence wind tunnel. We consider three different configurations: (i) the cable towed by itself; (ii) a light millimetric towed sphere made of expanded polystyrene; and (iii) a denser millimetric towed sphere made of lead. The trajectory of the cable tip is monitored using high-speed Lagrangian tracking, which allows one to characterize the average position and the dynamical fluctuations of the towed object. We show that the mean equilibrium position is well predicted by a simple model including the aerodynamical forces acting along the cable and on the towed sphere (when present). Concerning stability issues, we find that the heavy lead particle is always towed in stable conditions (within the accessible range of velocities) with only very low energy oscillations related to a weak pendulum-like motion. In contrast, the free end and light sphere cases are shown to become unstable when the towing velocity exceeds a certain threshold. Spectral analysis shows a *flutter*-type instability for the sphere, with a dominant oscillatory motion, while the cable alone develops a *divergence*-type instability with random fluctuations.

[1] Author to whom any correspondence should be addressed.

Content from this work may be used under the terms of the Creative Commons Attribution-NonCommercial-ShareAlike 3.0 licence. Any further distribution of this work must maintain attribution to the author(s) and the title of the work, journal citation and DOI.

© IOP Publishing Ltd and Deutsche Physikalische Gesellschaft

Contents

1. Introduction

The dynamics of towed objects in a fluid environment is of interest for many practical situations. For instance, acoustic streamers, where a sonar array is towed at the tip of a long cable attached to a ship or a submarine, are commonly used to detect and analyze sonic signals in the ocean [1]. Aerial systems towed by aircrafts were used for express mail delivery in the first half of the 20th century, and applications are still considered for precision payload delivery or snatch pick-up [2–4], aerial refueling (see figure 1) and low-altitude atmospheric research [5, 6], among others.

In the context of these applications, it is of crucial importance to warrant the stability of the trajectory of the towed object (at the tip of the cable), which turns to be an interesting and complex fluid dynamics problem. The dynamics of the towed object indeed results from several contributions: (i) the aero/hydro-dynamic forces exerted by the surrounding fluid (including primarily drag and lift but possibly also added mass effects and pressure gradients when the environment is turbulent, etc) directly on the object itself, (ii) the tension of the towing cable (which itself is subjected to aero/hydro-dynamic forces) and (iii) gravity. As a consequence, the towed object is coupled to the fluid both directly and also indirectly via the cable. Investigation of the coupling between the cable and the fluid is, therefore, also of crucial importance.

Existing investigations on towed systems are essentially numerical and investigate the stability of the system using lumped mass models for the cable [4, 7, 8], but a few systematic experimental investigations are available [9, 10]. The problem is also closely related to that of cylinders or elongated filaments in axial flows, which has been extensively investigated theoretically, numerically and experimentally [1, 11–17]. Most studies concern, however, cylinders with a moderate length-to-diameter ratio, for which it is now well established that in axial flows, the free end of the cylinder becomes unstable above a certain threshold of wind velocity. Several types of instability have been reported, including mainly divergence (which corresponds to a non-oscillatory motion with growing amplitude) and flutter (oscillatory motion) [11, 18]. Recently, Schouveiler *et al* [15] also reported flutter instability for a cylinder inclined in a flow. In both cases (a short cylinder in an axial or inclined flow), the instability is relatively well predicted numerically from the coupling between the fluid and the cylinder (via inviscid terms and friction) [19]. A more detailed review on the dynamics of flexible cylinders in flows can be found in [20].

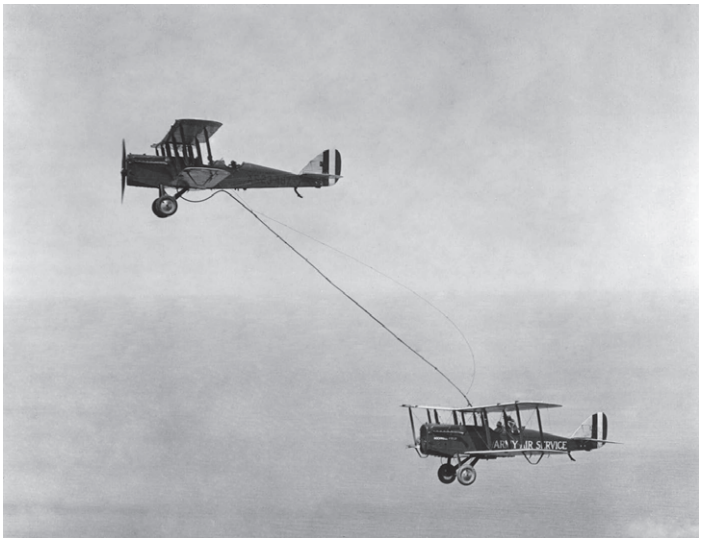

Figure 1. Aerial refueling is an example of a towed cable system for which stability issues are crucial for connecting maneuvers. The picture shows the first aerial refueling on 27 June 1923. (Source: US Air Force.)

The case of very long cylinders is of particular interest because most of the mentioned practical applications of towed systems do use long cables where the length-to-diameter ratio is large (cables towing acoustic streamers in the ocean can be kilometers long for a few centimeters in diameter). However, the study of the stability of such long cylinders in a flow remains an open field of theoretical and numerical research. The problem of long cylinders is particularly difficult to tackle theoretically and numerically due to the important scale separation related to the large length-to-diameter ratio and also to small-scale deformations induced by bending stiffness effects. A detailed discussion on this subject may be found in Langre and Paidoussis [16]. Using a string model, which neglects flexural rigidity, Triantafyllou and Chryssostomidis [21] found that a cable will always remain stable above a certain finite length-to-diameter ratio. Dowling [1] developed a different analysis, based on asymptotic expansion, and including flexural rigidity when necessary, but also concluded that long cylinders in axial flows should remain always stable. More recently, de Langre and Paidoussis [16] performed a finite element numerical resolution of the governing equation for long cables in axial flow, including effects of bending stiffness. Their results suggest that both *divergence* and *flutter* instability are possible for long cylinders. *Flutter* is found to develop as a secondary instability following *divergence* and its appearance is found to depend on the base drag at the free end of the cable. On the experimental side, characterization of the dynamics of long cylinders remains scarce, probably due to the difficulty of achieving appropriate conditions in laboratory facilities. The main works available are those realized by Ni and Hansen [14] and by Sudarsan *et al* [9] (with a length-to-diameter ratio of the cable of 500 and 150, respectively) for cylinders submerged in water. Both studies report *divergence* and *flutter* of the cylinders.

In this paper, we consider a towed system where the length-to-diameter ratio of the cable is 5×10^4, hence several orders of magnitude higher than in previous studies. The focus is put on analysis of the Lagrangian dynamics of the tip of the cable. The towing configuration is artificially obtained by considering a steady cable (with one fixed end and a free tip end to

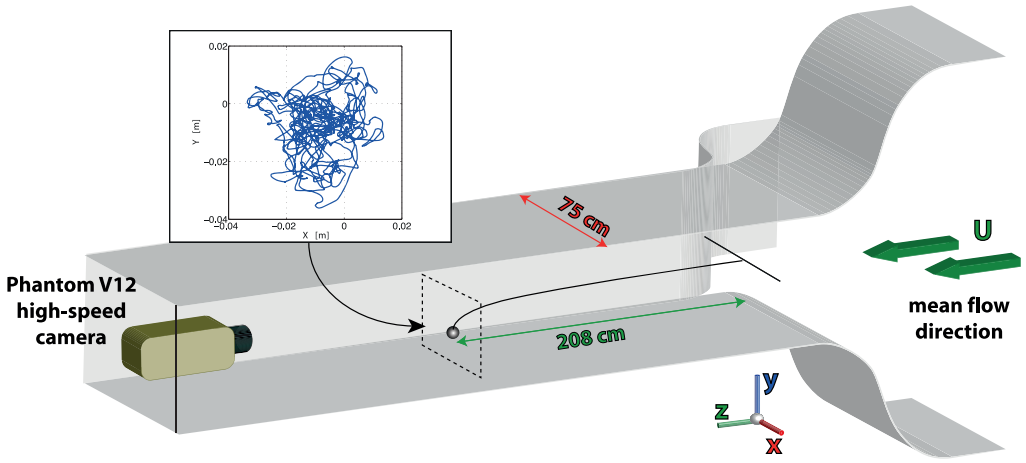

Figure 2. Sketch of the experimental setup. The inset shows an example of the fluctuating trajectory of the tip of the cable, recorded using a high-speed camera. The amplitude of the transverse motion is a few centimeters at most, and remains small compared to the length of the cable (2.08 m), so that the tip moves practically in a transverse plane ($x\,O\,y$), located around 2.1 m downstream of the entrance of the wind tunnel measurement section.

which a sphere is eventually attached) in a horizontal low-turbulence wind tunnel (see figure 2). This reproduces the situation of an object towed horizontally at constant speed (therefore we will indifferently use the terminology *wind velocity* or *towing velocity* in the subsequent). We consider three different configurations of a cable tip: (i) just the free end by itself (without any sphere attached); (ii) a light millimetric sphere made of expanded polystyrene; and (iii) a denser millimetric towed sphere made of lead. For each situation, a systematic study of the influence of the towing velocity on the equilibrium and stability of the cable extremity is conducted.

This paper is organized as follows. Section 1 describes the experimental setup (wind tunnel, cable characteristics, towed particles and the Lagrangian tracking technique); section 2 focuses on the investigation of the equilibrium position of the cable tip for the three cases (free end, polystyrene sphere and lead sphere); in section 3, we investigate fluctuations of the cable tip and address the problem of stability of its dynamics. Finally, a brief discussion of the observed behaviors is presented.

2. Experimental setup

The experiment has been run in a low-turbulence wind tunnel (figure 2), with a measurement section of $0.75\,\mathrm{m} \times 0.75\,\mathrm{m} \times 4\,\mathrm{m}$. The mean wind velocity, U, was varied in the range of 4–$15\,\mathrm{m\,s^{-1}}$, in which the tunnel operates in stable conditions with a fluctuation level below 5‰.

The towing cable is a thin polyamide–nylon fiber, with a lineal density of the order of $17\,\mathrm{mg\,m^{-1}}$, made of three stranded filaments with a diameter of $25\,\mu\mathrm{m}$ each. The resulting equivalent diameter for the stranded cable is of the order of $a_c = \sqrt{3} \times 25 \simeq 43\,\mu\mathrm{m}$. Table 1 summarizes the main physical properties of the cable. One extremity of the cable is fixed at the entrance of the test section at the center of the tunnel, while the other end is free to move. The fixed extremity of the cable is attached at the middle of a transverse horizontal *support*

Table 1. The main physical properties of the towed cable investigated.

Material	Length (L) (m)	Lineal density (mg m^{-1})	Elastic tension[a] (E_t) (GPa)	Elastic flexion (E_f) (GPa)	Flexural rigidity (EI) (Nm^2)	Poisson coeff. (ν)	Friction coeff.
Polyamide nylon 6,6	2.08	1.7	3.3	2.8	4.9×10^{-10}	0.41	0.2–0.3

[a] The corresponding global elastic stiffness for the considered cable, made up of three filaments of diameter $d = 25\,\mu$m and length $L = 2.08$ m, is $k = 3E_t(\pi d^2/4)/L \simeq 2.3$.

Table 2. Characteristics of the towed spheres investigated.

Material	Diameter (mm)	Density (kg m^{-3})	Re_p (min, max)
Free end (nylon)	$\sim$0.09	1140	$\sim$(10, 45)
Expanded polystyrene	6.3	13.35	(1680, 6300)
Lead	1.7	9130	(450, 1700)

cable tensed across the tunnel at mid-height and located at the entrance of the test section (see figure 2). The support cable must be as thin as possible in order to minimize perturbations of the flow; we use the same fiber with 43 μm of equivalent diameter and we have checked that no measurable increase of the natural fluctuation level of the flow in the wind tunnel was detected downstream due to the presence of the *support* cable. The fixed point is nearly at the center of the test section. The length of the towing cable is $L = 2.08$ m, which places the free tip nearly at mid-distance between the entrance and the exit of the 4 m long test section. Considering this length, which is significantly longer than the maximum transverse displacement of the tip (which does not exceed a few centimeters), the motion of the moving extremity of the cable is essentially two dimensional (2D), in a transverse xOy plane.

Three configurations were investigated for the moving end of the cable: a free end, an expanded polystyrene sphere and a lead sphere. For the case of the free end, a small single knot (with effective diameter $d_k \simeq 2a_c$), colored with red varnish, was made at the tip of the cable to improve its visualization. Note that in the following, we shall generically use the terminology *cable tip* or *cable end* although for the cases where a sphere is towed, this should be understood as *the sphere at the cable tip*. The parameters of the towed spheres are shown in table 2. We define the particle Reynolds number as $Re_p = Ud_p/\nu$, with d_p the sphere diameter and ν the kinematic viscosity of air (for the free end case, Re_p is estimated based on the cable equivalent diameter of 43 μm). The table also gives the range of Re_p spanned in each case as the wind velocity is varied from 4 to 15 m s^{-1}. We note at this point that due to the very small diameter of the cable (which is required to achieve the large aimed length-to-density ratio), the Reynolds number based on the cable diameter is orders of magnitude below that of most previous works and is below that of applications mentioned in the introduction. The main impact of this results in a necessity to consider non-trivial Reynolds number dependences of the several drag coefficients involved in modeling the cable–fluid interaction. This point will be further discussed in section 3.1.

The motion of the moving extremity of the cable is recorded using a Phantom V12 high-speed camera from Vision Research Inc. (New Jersey, USA). The spatial resolution used was of

768×600 pixels, with a repetition rate of 1000 fps. We recorded sequences of 18 500 images (corresponding to 18.5 s of continuous recording after which the 8 Gb on-board memory of the camera was full). To improve statistical accuracy 40 such acquisitions were taken for each mean velocity and each of the three towed systems investigated.

3. Results

3.1. Mean height

We first investigate the average equilibrium position of the cable tip as a function of the wind velocity for each configuration (a free end, a light towed sphere and a heavy towed sphere). The picture is qualitatively trivial: at zero velocity the tip lies on the floor of the tunnel test section; the tip *takes off* when the aerodynamic forces on the cable and towed object are sufficient to produce a vertical component surpassing the weight of the system; then as the velocity is increased, the cable tends to align with the main stream. Figure 4(a) shows the height y of the cable tip as a function of the wind speed U for the three configurations ($y = 0$ m corresponds to the particle being on the floor of the tunnel). As we will see in the next subsection, for large wind velocities the dynamics of the cable end may become highly fluctuating. In this section, we investigate the average vertical position of the cable tip. For the free end and for the light polystyrene particle, it can be seen that as the velocity increases the average height reaches an asymptotic value corresponding to the height of the fixed end of the cable ($y_0 \simeq 0.4$ m), which is then aligned with the horizontal mean stream. For these *light* towed objects, the tip of the cable has already *taken off* even for the lowest wind velocities investigated. The heavy lead particle, in contrast, is found to *take off* only when the wind velocity exceeds a threshold of the order of $6\,\mathrm{m\,s^{-1}}$. We also note that for this heavy towed particle, the highest velocity investigated is not sufficient to reach the asymptotic horizontal cable limit.

As already mentioned, the *take off* of the towed objects results from mainly two contributions: (i) the aerodynamic drag acting on the cable, which tends to rise globally the cable and the object at its tip, and (ii) the aerodynamic drag acting on the towed sphere (when present), whose reaction on the cable tends to enhance the horizontal component of the tension at the tip and hence to flatten the cable horizontally. Dowling [1] has derived the system of equations governing the average cable position, based on the tension average amplitude $\overline{T}(l)$ and on its local average angle $\overline{\theta}(l)$ (defined with respect to the mean stream) along the cable length. By considering the tangential and perpendicular equation of motion of an elementary element of cable (see figure 3 for a schematic representation of the forces acting on the cable at equilibrium), the following system of equations can be obtained for the equilibrium tension and local angle (details of the derivation of these equations can be found in [1]):

$$\begin{cases} \dfrac{\partial \overline{T}}{\partial l} = -\rho_0(\sigma - 1)\pi a_c^2\, g \sin(\overline{\theta}) - \rho_0 U^2 \pi a_c C_T \cos(\overline{\theta}), \\ \overline{T}\dfrac{\partial \overline{\theta}}{\partial l} = -\rho_0(\sigma - 1)\pi a_c^2\, g \cos(\overline{\theta}) + \rho_0 U^2 a_c (C_D \sin(\overline{\theta}) + \pi C_N) \sin(\overline{\theta}), \end{cases} \tag{1}$$

where l denotes the curvilinear coordinate along the cable ($l = 0$ corresponds to the fixed end and $l = L$ to the cable tip), ρ_0 is the density of air, σ is the specific density of the cable, a_c is the equivalent cable diameter (here taken as $a_c = 43.3\,\mu$m), C_T is the tangential frictional

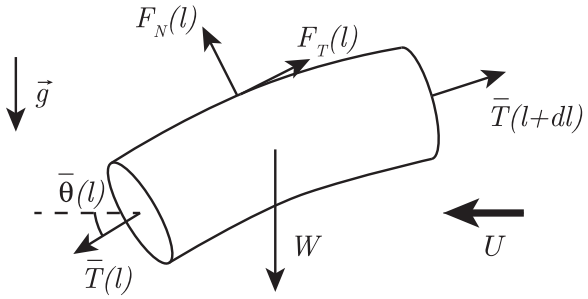

Figure 3. Schematic representation of the forces acting on an elementary element of a cable of length dl. $\overline{T}(l)$ is the tension along the cable; $F_{\mathrm{N}}(l) = 1/2\rho_0 a_{\mathrm{c}} U^2 (C_{\mathrm{D}} \sin^2 \overline{\theta}(l) + \pi C_{\mathrm{N}} \sin \overline{\theta}(l))$ is the normal lineal aerodynamic force (frictional+pressure drag) [1]; $F_{\mathrm{T}}(l) = 1/2\rho_0 \pi a_{\mathrm{c}} U^2 \cos \overline{\theta}(l)$ is the tangential lineal aerodynamic force (frictional drag) [1]; $\vec{W} = \rho_0(\sigma - 1)\pi/4\, a_{\mathrm{c}}^2 \vec{g}$ is the lineal net weight of the element. Note that for the stationary equilibrium analysis, where no acceleration of the cable relative to the fluid is considered, added mass effects are not included.

drag coefficient, C_{N} is the normal frictional drag coefficient and C_{D} is the pressure drag coefficient [22].

This system of equations has then to be completed with an appropriate set of boundary conditions to be applied at the extremity of the cable. When the cable is towed by itself (with no object trailed at its end), this condition is simply $\overline{T}_{\mathrm{tip}} = 0$ (as the tension vanishes then at the free end of the cable). It can be shown in this case that the shape of the cable is a straight line, with the angle $\overline{\theta}(l)$ remaining constant along the cable length ($\frac{\partial \overline{\theta}}{\partial l} = 0$) at a critical value θ_{c} [1, 23]. Then the critical angle can be simply obtained from the boundary condition $\overline{T}_{\mathrm{tip}} = 0$, applied to the transverse equation in system (1), as the root of the equation

$$-\rho_0(\sigma - 1)\pi a_{\mathrm{c}}^2\, g \cos(\overline{\theta}_{\mathrm{c}}) + \rho_0 U^2 a_{\mathrm{c}} (C_{\mathrm{D}} \sin(\overline{\theta}_{\mathrm{c}}) + \pi C_{\mathrm{N}}) \sin(\overline{\theta}_{\mathrm{c}}) = 0. \tag{2}$$

When the cable does tow an object at its end, the appropriate boundary condition is given by the balance of the forces acting on the towed particle at the tip (this boundary condition accounts for the contributions coming from the aerodynamic forces acting on the particle):

$$\begin{cases} \overline{T}_{\mathrm{tip}} \cos \overline{\theta}_{\mathrm{tip}} = \dfrac{\pi}{8} d_{\mathrm{p}}^2 C_{\mathrm{p}} U^2, \\ \overline{T}_{\mathrm{tip}} \sin \overline{\theta}_{\mathrm{tip}} = m_{\mathrm{p}} g \end{cases} \tag{3}$$

with d_{p} the diameter of the towed particle, m_{p} its mass and C_{p} its drag coefficient.

We have solved the system of equations (1) with the appropriate boundary conditions for the three towing configurations, for mean wind velocities U varying within the accessible experimental range. The height of the cable is then derived from the resulting calculated profile of the cable shape. Note that solving these equations requires knowledge of several parameters, in particular, the drag coefficients of the particle C_{p} and of the cable C_{T}, C_{N} and C_{D}. The drag coefficient for spherical particles is well tabulated (see, for instance, [22, 24]), so we have used the commonly accepted values according to the particulate Reynolds number of our particles. In the range of velocities explored, this coefficient is essentially constant and equal to $C_{\mathrm{p}} \simeq 0.5$; however, for each velocity and particle diameter, we estimate the drag

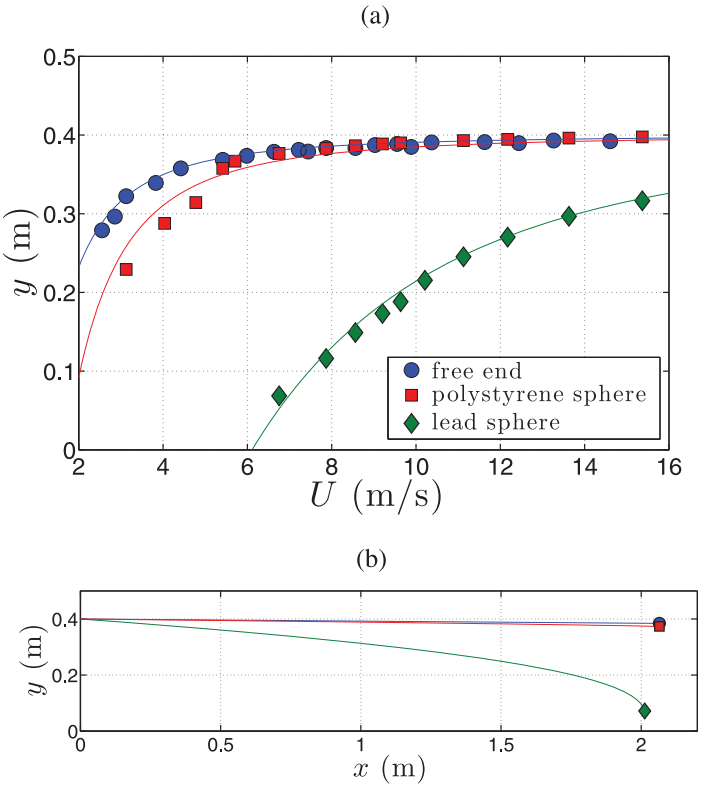

Figure 4. (a) The mean height for the wire cable tip measured for the three configurations of the towed object. The dashed lines correspond to the best simultaneous adjustment of the drag coefficients C_D, C_N and C_T acting on the cable in equations (1). (b) Global shape of the cable calculated from the resolution of equations (1).

coefficient precisely according to well-established empirical formulae [24]. Concerning the cable coefficients, it should be noted that the Reynolds number based on the equivalent diameter of the cable varies in the range $10 < Re_c = a_c U/\nu < 45$ when the mean wind velocity U is varied between 4 and 15 m s^{-1}. In this relatively low Reynolds number regime, the drag coefficients of the cable have a non-trivial dependence on Reynolds number [22]. The behaviors of C_T and C_D are relatively well documented for cylinders, cables and wires [22, 25]. In the present range of interest the Reynolds number dependence of C_T and C_D is well approximated by power laws

$$C_{T,D} \simeq A_{T,D}\, Re_p^{\alpha_{T,D}}, \tag{4}$$

where we have determined $A_T = 10$, $\alpha_T = -0.76$, $A_D = 7.6$ and $\alpha_D = -0.43$, based on the data in [25]. Values for C_N are much less documented, although it is generally accepted that $0 < C_N < C_T$ [1, 26]. Therefore, C_N is used as a fitting parameter to adjust the theoretically calculated height and the experimental measurements. More precisely, a power-law dependence $C_N = A_N Re_p^{\alpha_N}$ is also assumed and we use the two fitting parameters A_N and α_N. We stress that these two parameters are simultaneously fitted, at once from the experimental data shown in figure 4(a) for the three configurations (a free end, a polystyrene sphere and a lead sphere). The solid lines represented in figure 4(a) show the corresponding best fit, which is obtained for $A_N = 0.8$ and $\alpha_N = -0.12$. We found very good agreement between the simple theoretical

approach and our measurements. Besides, we note that being able to simultaneously fit the three configurations with a single set of fitting parameters is particularly satisfactory with regard to the relevance of the model and of the estimation of the various parameters involved (in particular, C_p, C_T and C_D).

As an example, figure 4(b) illustrates the corresponding shape of the cable calculated from the solution of equations (1) using these best fitting parameters for a towing velocity $U = 7\,\mathrm{m\,s^{-1}}$. Although we do not have at present the possibility of accurately measuring in our experiment the global shape of the cable, the calculated profiles shown in figure 4(b) are qualitatively consistent with the visual inspection of the cable. In particular, the cable is observed to be nearly straight for the case with no sphere at the end and when the light polystyrene sphere is towed, while it is clearly curved for the heavy sphere case.

3.2. Dynamical fluctuations and stability

In this section, we report on the statistics of velocity fluctuations of the towed bodies. We first describe the dependence on experimental parameters of velocity standard deviation of the cable tip motion, before discussing its spectral properties.

3.2.1. Velocity fluctuations. Figure 5 shows the standard deviations of the cable tip velocity for each towing configuration. Figure 5(a) corresponds to the free end case, figure 5(b) to the light polystyrene particle and figure 5(c) to the heavy lead particle. For each configuration the plot shows the dependence of the standard deviations of horizontal and vertical velocity components (σ_{v_x} and σ_{v_y}) on the towing velocity U. For comparison purposes, the range of the vertical axis has been kept identical for the three plots.

The free end case. We first analyze the results of the velocity of the tip of the cable alone, without any sphere attached. Interestingly, the level of fluctuations remains almost null below a threshold of wind velocity of the order of $U^* \simeq 6$–$7\,\mathrm{m\,s^{-1}}$. Above this threshold the tip of the cable becomes unstable and fluctuations of velocity are observed to grow as the mean wind speed is increased. It can be argued, based on the data reported on this plot, that the instability threshold might be slightly lower for the vertical component than for the horizontal one. Moreover, fluctuations of velocity exhibit a small (but measurable) anisotropy with higher fluctuations in the horizontal component far above threshold. It is also enlightening to compare the level of fluctuation of the cable tip with the natural small fluctuations of the flow itself. This is shown in the inset in figure 5(a), which represents the ratio of standard deviation of the cable tip velocity to that of the streamwise velocity of the flow itself $\sigma_{v_x,v_y}/\sigma_U$. As can be seen in this graph, the level of fluctuations of the cable tip velocity is about six times larger than the ambient fluctuations of the flow at the highest mean velocities investigated. This indicates that the instability of the tip dynamics is not related to possible reminiscent fluctuations of the flow (we recall that the turbulence level of our tunnel is very small and of the order of a few per thousand only).

Polystyrene sphere. The light sphere exhibits a similar dynamical behavior compared to the free end case just described: the fluctuation level is low as soon as the mean wind velocity remains below 5–$6\,\mathrm{m\,s^{-1}}$ and increases above that threshold. The typical amplitude of velocity fluctuations is slightly larger than that of the free end, but remains of the same order of magnitude. A clear difference concerns the almost perfect isotropy of the fluctuations of the sphere compared to the free end.

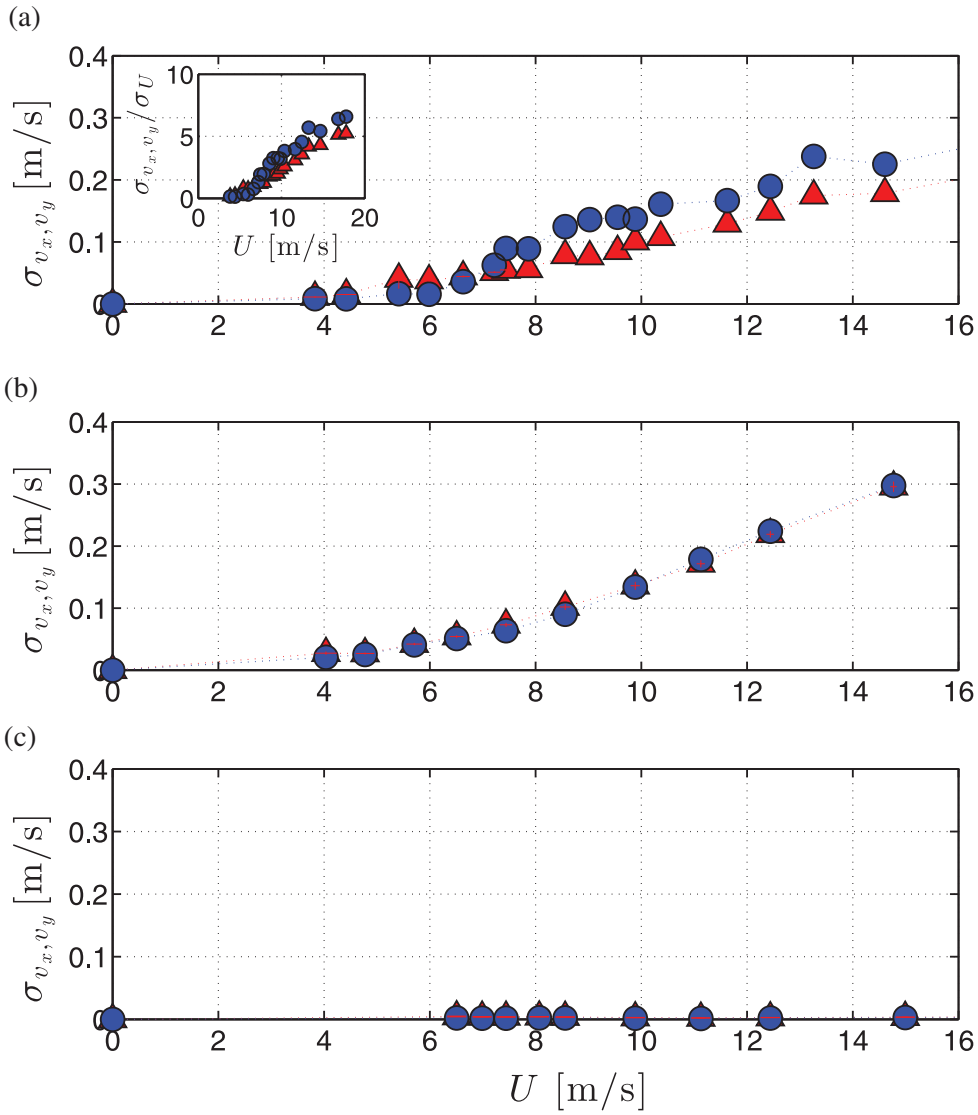

Figure 5. Experimental values of the standard deviations of the horizontal (blue circles) and vertical (red triangles) components of the cable tip for three configurations: (a) a free end, (b) a polystyrene sphere and (c) a lead sphere. The inset in panel (a) shows the same data as the main graph, with the velocity standard deviations of the cable tip normalized by that of the carrier flow itself.

Heavy sphere. The dynamical behavior of the heavy sphere is clearly different from the previous cases. The fluctuation level is about two orders of magnitude lower than that of the polystyrene sphere or the free end. It is also one order of magnitude below the natural fluctuation level of the flow. It is therefore concluded that the heavy sphere is always towed in stable conditions.

3.2.2. Spectral analysis. Further insight can be obtained into the dynamics of the towed system by exploring the Lagrangian power spectral density (PSD) of the velocity as a function of the frequency component f for each configuration.

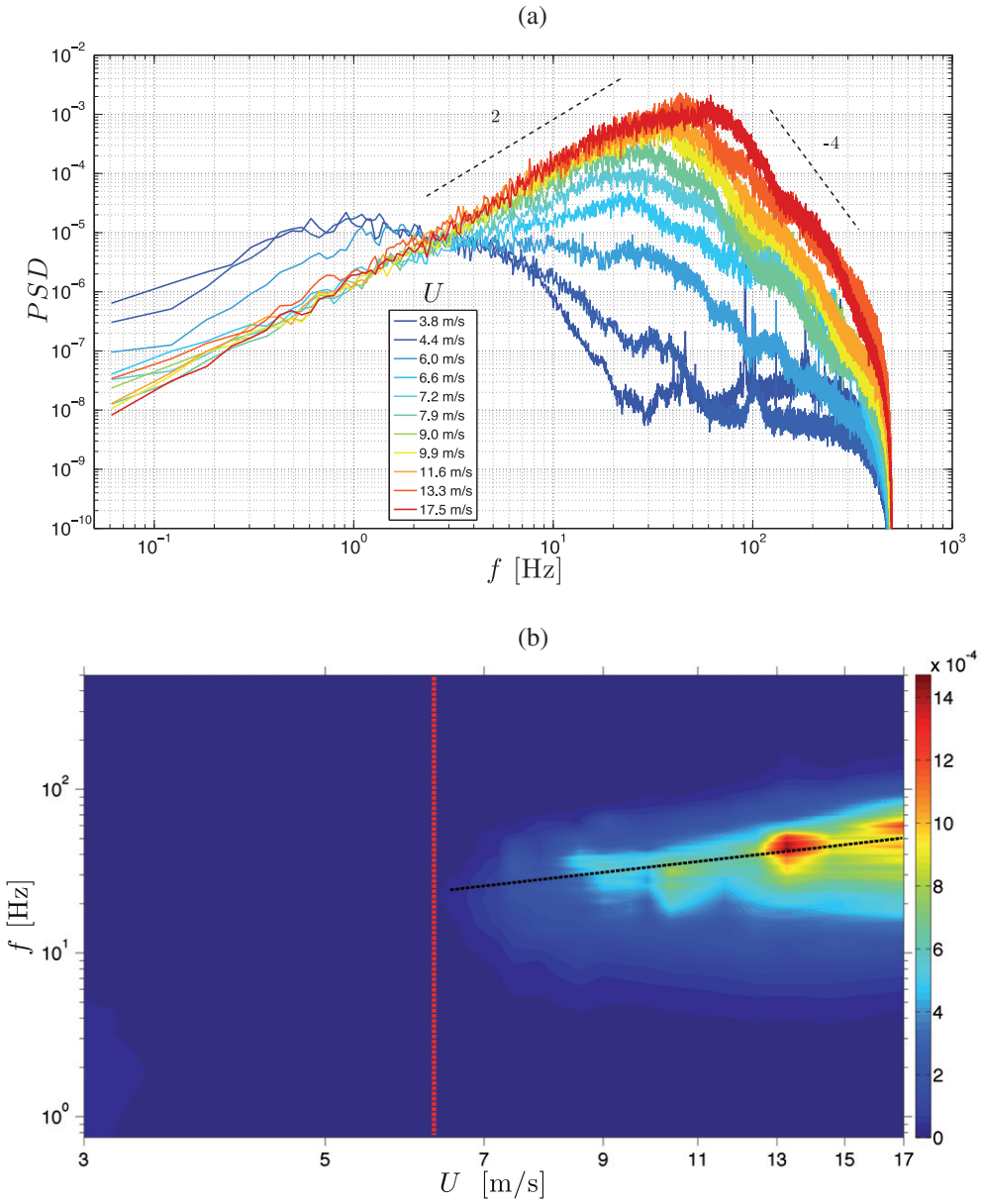

Figure 6. (a) PSD of the velocity fluctuations measured for a cable tip with no towed sphere (only the horizontal component is shown). The color codes the mean wind velocity, with the lowest in blue and the highest in red. (b) Interpolated representation of the previous PSDs in the velocity–frequency $(U-f)$ plane. The color codes the amplitude of the spectra in a logarithmic scale.

The free end case. Figure 6(a) shows the PSDs of horizontal velocity for the free end case at the different mean wind velocities investigated (vertical component exhibits almost identical spectral features). All the spectra naturally vanish at zero frequency, which reflects the absence of any mean drift velocity of the tip of the cable that simply wiggles around its average position. The low-frequency regime shows a clear f^2 law, consistent with a flat spectra for the long-term uncorrelated random displacement of the tip (note that the PSD of the displacement x is simply

related to that of velocity v_x by a factor of $1/(2\pi f)^2$). A remarkable feature of figure 6(a) is the trend of the spectra to exhibit a clear maximum as the wind velocity U increases. The amplitude and the peak frequency f_{pk} increase with U. It can be observed that the first hint of emergence of the spectral peak appears for a mean wind velocity between 6 and 7 m s^{-1}, which is comparable with the threshold velocity U^* for which the standard deviation of velocity for the free end was previously noted to start growing. The low frequency f^2 regime holds all the way below the maximum ($f < f_{pk}$). Above the peak ($f > f_{pk}$), the spectral power density decreases rapidly as f^{-4}, indicating an efficient dissipative mechanism of high-frequency fluctuations (very likely due to internal viscoelasticity [27], which is known to be important in polymer filaments). We stress that this broad spectral peak does not correspond to an oscillatory mode of the cable tip. Indeed, the corresponding spectra for the particle displacement remain flat for ($f < f_{pk}$) and are damped as f^{-6} for ($f > f_{pk}$). Hence at the instability onset, the cable tip simply wiggles randomly with no characteristic frequency and the peak frequency f_{pk} is simply related to the high-frequency dissipative cut-off.

The onset of the instability of the cable tip is better observed in figure 6(b) where we show a 2D interpolation of the spectra in figure 6(a) in the $(U-f)$ plane (20 measurements for different values of the mean wind speed, between 4 and 15 m s^{-1} were used to obtain this interpolation). This representation clearly shows that the tip of the cable becomes unstable for $U \gtrsim 7$ m s^{-1}, with a dominant frequency f_{pk} which increases with U as qualitatively illustrated by the dashed line in figure 6(b).

Polystyrene sphere. The same spectral analysis for the velocity of the light towed sphere shows some similarities but also clear distinctions compared the free end case. Figure 7(a) shows the PSDs for the light sphere towed at different mean velocities. As for the free end, at low frequencies, the velocity PSDs follow a f^2 regime, again consistent with a fully uncorrelated long-term dynamics of the sphere displacement. At high frequencies, a steep f^{-4} damping regime is also observed for the highest towing velocities U (although the damping is slightly less steep for the lowest towing velocities). As for the free end case, we observe the growth of a clear peak above a threshold mean wind velocity of the order of 5–6 m s^{-1}. However, the peak is much sharper and clearly defines a resonant frequency f_{pk}. The first hint of such a resonant peak, identifiable by the appearance of an inflection point prior to the spectral maximum, occurs for a wind velocity around $U^* \simeq 5.7$ m s^{-1}. This threshold is consistent with the growth of velocity standard deviation reported previously. We also note that above this threshold the amplitude of the resonant peak starts to exceed the maximum amplitude of the low velocity spectrum. The sharpness of the resonant peak can be quantified by its quality factor $Q = f_{pk}/\delta f$, where δf is the 3 dB bandwidth. This is shown in the inset of figure 7(a), which shows that Q exceeds 1 and grows sharply above U^* until it saturates around $Q \simeq 3.5$ for the highest velocities explored. These observations indicate that the instability of the towed sphere operates via an oscillatory mode. The amplitude and frequency of the unstable mode increase with the mean velocity U. We also note that above threshold, the spectral signature of the dynamics of the sphere for frequencies slightly below the resonant peak is much richer than that of the free end case. The resonance is indeed preceded by a plateau of random velocity fluctuations and the f^2 regime is only recovered at the very lowest frequencies (typically for slow fluctuations below 1 Hz). Finally, we note that as for the free end case, the growth of the sphere instability is well illustrated by the interpolated data in the $(U-f)$ plane, shown in figure 7(b).

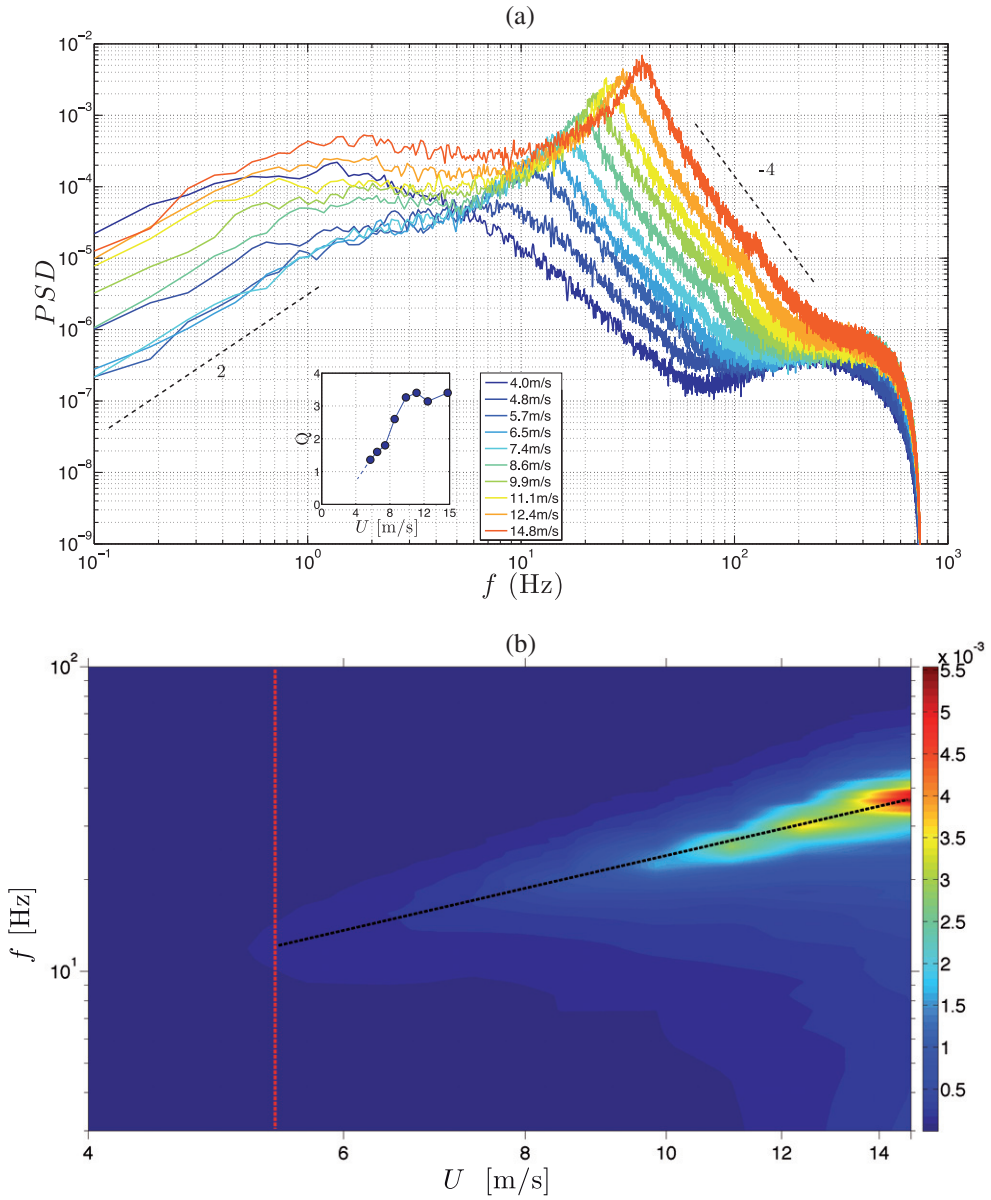

Figure 7. (a) PSD measured for the velocity fluctuations for the towed polystyrene sphere at different towing speeds (only the horizontal component is shown). The color codes the mean wind velocity, with the lowest in blue and the highest in red. The inset shows the quality factor Q of the resonant peak above the threshold instability. (b) Interpolated representation of the previous PSDs in the velocity–frequency ($U-f$) plane. The color codes the amplitude of the spectra.

Heavy sphere. The spectral analysis of the velocity of the heavy sphere reveals a completely different landscape. Figure 8(a) shows the spectra of the horizontal dynamics for the heavy towed sphere (again, the vertical component exhibits a similar behavior). This dynamics is clearly dominated by slow fluctuations with a resonant frequency peak f_{pk} around 1 Hz, which

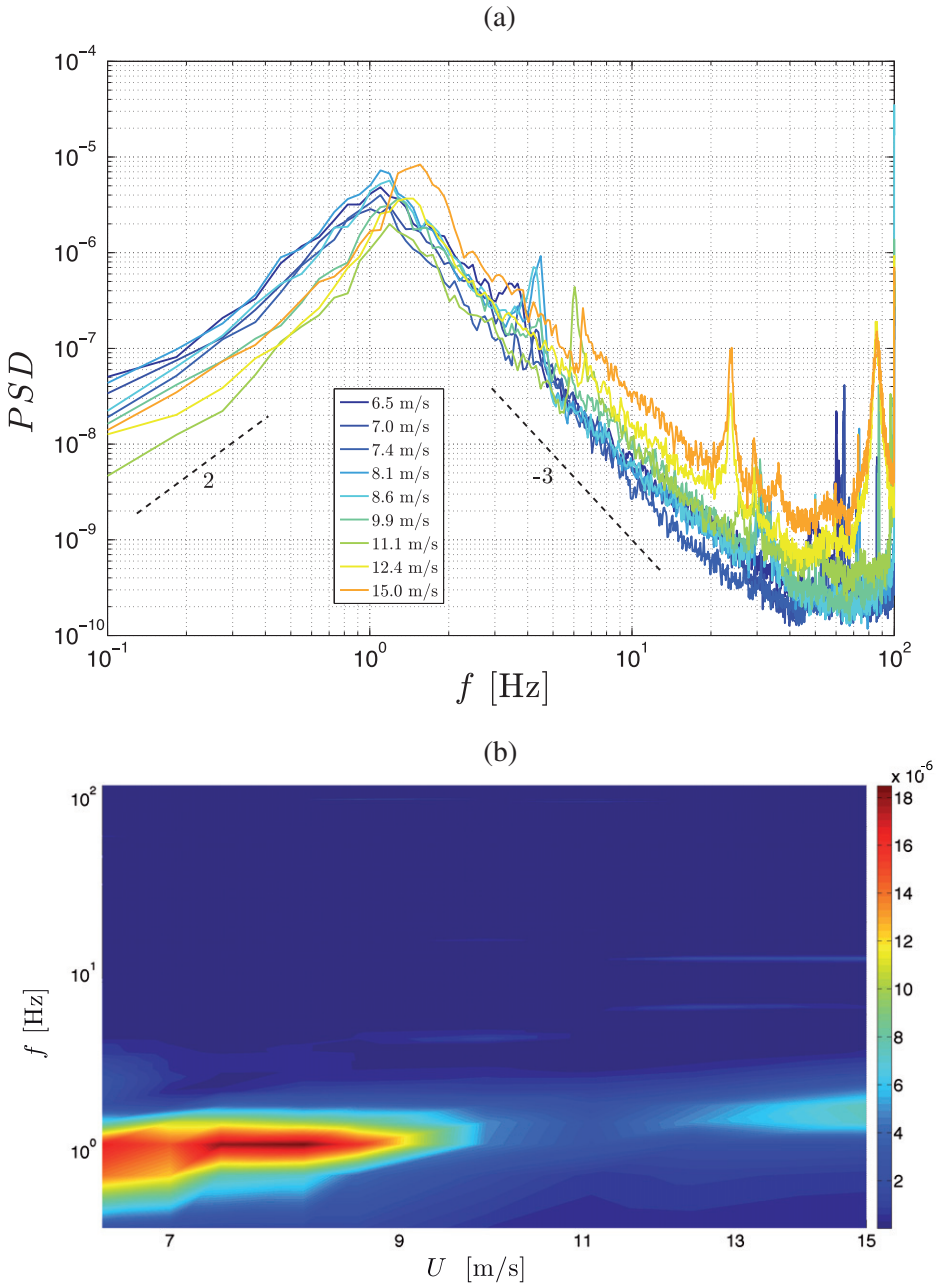

Figure 8. (a) PSD of the velocity fluctuations for the heavy sphere at different towing speeds (only the horizontal component is shown). (b) Interpolated representation of the previous PSDs in the velocity–frequency ($U-f$) plane. The color codes the amplitude of the spectra.

increases with the mean towing velocity U. At low frequencies the spectra follow an f^2 regime, although our measurements barely resolve the slowest fluctuations in this case (this is limited by the on-board memory of the camera, which limits the total length of the recorded trajectories to slightly less than 20 s). The high-frequency damping seems to be less steep than for the free end and light sphere case and roughly follows an f^{-3} regime. Several narrow peaks are

also observed for frequencies above f_{pk}, which are probably related to spurious noise (we point out that for consistency reasons, we used the same optical magnification for imaging the three configurations; hence the lesser amplitude of fluctuations of the heavy particle inevitably decreases the signal to noise ratio).

To finish the spectral analysis description, we show in figure 9(a) the power spectral densities at a given towing velocity (here $U \simeq 11\,\mathrm{m\,s^{-1}}$) for the three configurations. This graph is instructive in comparing the dynamics of the three situations:

- Although the standard deviations of the velocity of the free end and the light particle were found to be of the same order of magnitude in figure 5, the PSDs in figure 9 show that this results from a spurious compensation effect: slow fluctuations are orders of magnitude larger for the light sphere, while rapid fluctuations are stronger for the free end. For the towed light sphere case, more than 50% of the fluctuating energy comes from the narrow 3 dB bandwidth around the resonant peak (which corresponds to a band $\delta f \in [22; 29]\,\mathrm{Hz}$ for the data shown in figure 9).
- The global amplitude of PSD is orders of magnitude lower for the heaviest sphere, which was already illustrated by the standard deviations of velocity, σ_v, previously discussed (we recall that the variance σ_v^2 of the velocity is simply given by the integral of the PSD).
- The peak frequency of the heavy particle appears to be much lower than that of the free end and the light sphere.

Finally, figure 9(b) shows the dependence of the frequency peaks on the towing velocity U for each case. The free end case and the heavy particle case are well described by a linear law where $f_{pk} \propto U$, whereas the resonant frequency for the polystyrene particle increases slightly faster and is better described by a power law $f_{pk} \propto U^{1.2}$.

3.3. Discussion

The previous observations show that the dynamics of the free end and that of the light towed sphere become unstable above a certain threshold (which is comparable for both situations and of the order of $6\,\mathrm{m\,s^{-1}}$). However, while the simple analysis of velocity standard deviations may have suggested similar dynamics for both cases, the spectral analysis has revealed clearly different dynamical landscapes. The heavy particle is, in contrast, found to be always towed in stable conditions. In the following paragraphs, we briefly discuss some of these observations.

3.3.1. Pendular motion of the heavy sphere case. Let us first discuss the case of the heavy particle. During the experiment, a pendular motion of the sphere, with a relatively short effective pendulum length (compared to the cable length) can be visually observed in the tip region of the cable. We argue here that the peak observed in the spectrum of the heavy particle is reminiscent of this slow pendulum-like motion. The order of magnitude of the pendular oscillation frequency can be estimated based on a very crude model illustrated as shown in figure 10. The profile of the cable is qualitatively approximated by two linear pieces obtained from the tangents at the fixed point and at the tip of the cable, estimated from the calculated equilibrium profile (as shown, for instance, in figure 4(b)). As shown in figure 10, in this crude approximation, the effective length l_{eff} of the pendular motion of the sphere at the tip of the cable represents a fraction of $(y_0 - y_s)$, where y_s is the height of the sphere and $y_0 \simeq 0.4\,\mathrm{m}$ is the vertical ordinate of the cable fixed end.

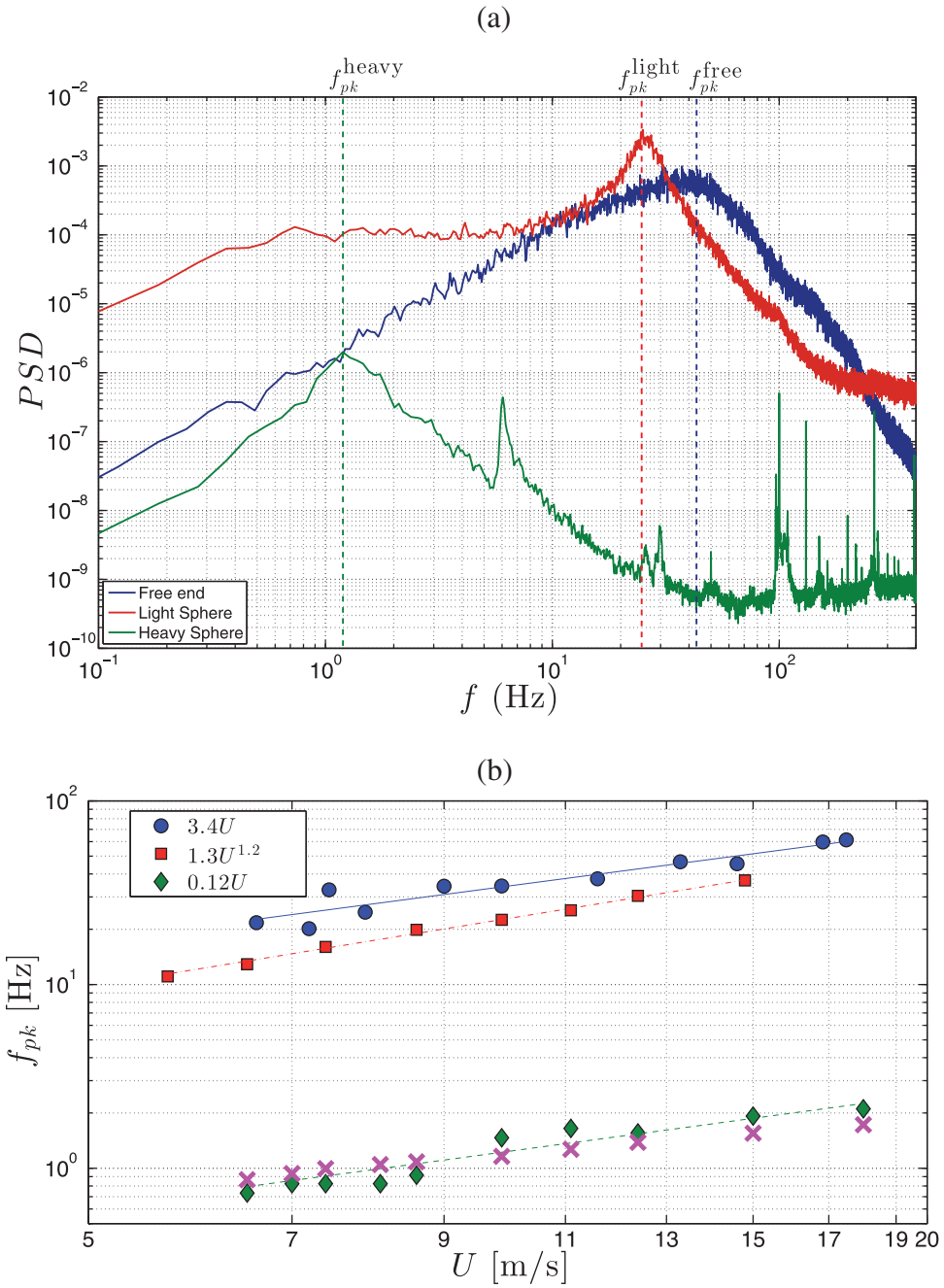

Figure 9. (a) Comparison of the spectral densities for the three towed configurations (a free end, a light particle and a heavy particle) at a given towing velocity $U \simeq 11\,\mathrm{m\,s^{-1}}$. (b) Dependence of the peak frequency on mean towing velocity U for the three configurations: a free end (blue circles), a polystyrene sphere (red squares) and a lead sphere (green diamond). The lines indicate the best power-law fit whose parameters are given in the legend (note that linear fit indeed corresponds to a power-law fit for which the best fitting exponent was found to be almost 1). Magenta crosses indicate the estimation of the peak frequency for the heavy lead particle based on a simple pendular model discussed in section 3.3.

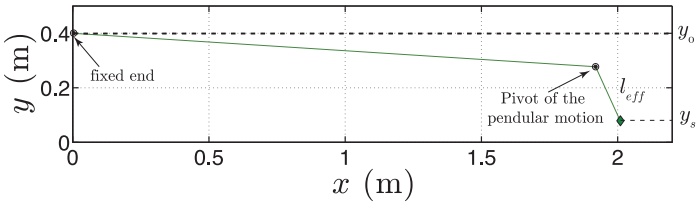

Figure 10. Simple pendulum model for the heavy particle, where the profile shown in figure 4(b) is crudely approximated by the two tangents (at the fixed end and at the tip of the cable). The pivot of the pendular motion at the tip of the cable is taken at the intersection of these two lines.

For the sake of simplicity in estimating the order of magnitude of the oscillation frequency, we approximate $l_{\mathrm{eff}} \simeq (y_0 - y_s)/2$. The expected frequency for the pendular motion at the tip of the cable can then be estimated as

$$f_0 = \frac{1}{2\pi}\sqrt{\frac{g}{l_{\mathrm{eff}}}} \simeq \frac{1}{2\pi}\sqrt{\frac{2g}{y_0 - y_s}} \tag{5}$$

with g the gravity acceleration. The green crosses in figure 9(b) present the corresponding estimate based on the actual measurement of the sphere height y_s shown in figure 4(a). In spite of the crudeness of the model, very good agreement is found. The model can certainly be improved by a better piecewise decomposition of the cable, but this simple analysis seems to confirm the pendular origin of the observed spectral peak.

We point out, however, that except for this pendular motion, the dynamics of the heavy particle remains stable with a level of fluctuation much lower than the free end and polystyrene sphere cases, as shown in figure 4(a). The stabilizing effect of a heavy mass on the dynamics of towed cables is a well-known property in the underwater community. Adding a weight depressor in two-part towing system has become a common strategy to reduce the instability of underwater towed systems [28].

3.3.2. Divergence instability of the towed cable. Concerning the free end case, where the cable is towed by itself, our results are worth discussing in comparison with recent numerical simulations of long cylinders in axial flow by Langre and Païdoussis [16], which we briefly summarize first. Their simulations are the first to show that, contrary to previous predictions [1, 21], long cylinders may become unstable. The existence of the instability for such long cylinders requires bending stiffness effects to be correctly included in the model. It is indeed directly related to the presence of a *neutral point* in the cable at which base drag, axial compressive forces and tangential friction balance. Upstream of the *neutral point*, the cable is in tension due to the frictional drag along its length, which plays a stabilizing role. Downstream of the *neutral point*, the cable is in compression, and no stiffness exists other than flexural rigidity, which then needs to be correctly modeled. The position of the *neutral point* along the cable is $x_c = L - L_c$, with [1, 16]

$$L_c = \frac{a_c}{2C_T}(\pi - 2C_b), \tag{6}$$

where C_b is the base drag coefficient at the tip of the cable (defined such that $F_{BD} = 1/2\rho D^2 U^2 C_B$ is the base drag force). A necessary condition for the instability to appear is that $x_c < L$ (so that the *neutral point* is actually *in* the cable), which requires $C_b < \pi/2$ (i.e. the cable tip must be sufficiently streamlined). More precisely, de Langre and Païdoussis have shown that the instability diagram (see, for instance, figure 6 of [16]) depends mainly on two parameters: (i) the shape of the downstream end of the cable (characterized by a parameter $f \in [0; 1]$ related to base drag and lift coefficients at the tip of the cable (de Langre and Païdoussis use the ad hoc empirical relation $f = 1 - 4C_b/\pi$); it is such that $f = 0$ for blunt cylinder tips and $f = 1$ for perfectly streamlined tips) and (ii) the ratio C_N/C_T (the range of C_N/C_T investigated by de Langre and Païdoussis is [0.5 ; 1.5]). They find that long blunt cables ($f \to 0$) remain always stable. Above a certain threshold of f (which depends on C_N/C_T, but which is typically of the order of $f \sim 0.5$), i.e. for sufficiently well-streamlined cable tips, a *divergence* instability appears. The typical predicted velocity threshold U_d^* for *divergence* is of the order of some meters per second in the range of parameters they investigated. If f is further increased (the tip becoming even more streamlined) a secondary bifurcation may develop, from *divergence* to *flutter* (the motion of the cable then becomes oscillatory). Results of de Langre and Païdoussis also show that for long cylinders stability analysis becomes independent of the cable length, and only a short portion at the downstream end of the cable is concerned. The length of the unstable portion is given by L_c.

A direct quantitative comparison of these numerical results with our experiments is difficult due to the impossibility to exactly match the parameters of the simulation to that of the experiment. The ratio C_N/C_T in the experiment can be estimated from the fitted Reynolds number dependence for C_N and C_T discussed in section 3.1. We find it to vary from 0.2 to 1.1 as the flow velocity increases from 4 to 20 m s^{-1} typically. It is therefore in a comparable range to that explored by de Langre and Païdoussis. Estimation of parameters f and C_b (characteristic of the tip shape of the cable) in the experiment are more subtle and will be discussed below. It is first interesting to note that several results of de Langre and Païdoussis are in good qualitative agreement with our experiment.

1. We do observe in the experiment a transition toward a *divergence*, non-oscillatory instability. The instability appears above a velocity threshold of the order of 6–7 m s^{-1}.
2. Visual inspection of the cable shows that only a short portion (a few centimeters long) at the downstream end of the cable is destabilized.
3. We have carried out a few extra experiments, identical to what was presented above but increasing the length of the cable up to 3.5 m. These measurements confirm that the dynamics of the cable tip is independent of the cable length. In particular, instability threshold and PSDs of the cable tip motion are indistinguishable for the two lengths.

A more quantitative discussion requires us to estimate the base drag coefficient C_b (which controls the position of the *neutral point* on the cable). The presence of the small knot used to visualize the cable tip makes this estimation non-trivial. When examined under a magnification lens, the knot appears as a deformed sphere with diameter of the order of $d_k \simeq 2a_c$. The base drag coefficient C_b can be related to the knot drag coefficient C_k by $C_b = \pi/4(d_k/a_c)^2 C_k$ (approximating the projected area of the knot as $\pi d_k^2/4$). Considering the low value of the Reynolds number $Re_k = U d_k/\nu$ and approximating C_k by the drag coefficient of a sphere of diameter d_k, we can estimate $C_k \simeq 24/Re_k$. Hence, the base drag coefficient can be estimated as

$C_b \simeq \frac{6\pi\nu}{U d_k} (d_k/a_c)^2$. The condition $C_b < \pi/2$ for the neutral point to be in the cable then requires

$$U > U^* = \frac{12\nu}{a_c^2} d_k. \tag{7}$$

Using the values $a_c = 43\,\mu$m and $d_k = 2a_c$ leads to $U^* \simeq 8$ m s. Considering the several approximations (in particular, regarding the spherical shape of the knot and the estimation of C_k) this value is in good agreement with the measured threshold (6–7 m s^{-1}). It suggests that the appearance of *divergence* in our experiment is concomitant with the appearance of a neutral point in the vicinity of the downstream end of the cable.

Finally, we note that we do not observe in our experiment any secondary bifurcation toward *flutter* when the cable is towed without any sphere attached. A possible explanation for that may be also related to the small knot at the tip of the cable. This tends to make the tip of the cable not very well streamlined and hence not suitable for *flutter* according to the de Langre and Païdoussis results.

3.3.3. Oscillatory instability of the light towed sphere. An oscillatory instability is, however, found when a light sphere is towed at the tip of the cable. The frequency of the observed oscillations increases from 10 Hz to about 40 Hz in the range of wind velocities explored above the instability threshold (from 5 to 15 m s). It is enlightening to note that this range of frequencies is inconsistent with simple mechanisms such as vortex shedding, pendular motion of the sphere, vibrating eigenfrequencies or elastic oscillations:

- *Vortex shedding.* In the range of Reynolds number considered for the sphere ($Re_p = d_p U/\nu > 2000$, above the instability threshold), its Strouhal number can be considered as constant and of the order of $St \simeq 0.2$. The vortex shedding frequency $f_p^{shed} = St\, U/d_p$ should therefore exceed 120 Hz for wind velocities above 4 m s^{-1}. Such high frequencies are in the damped region of the spectra of the particle motion (see figure 7(a)), and have not been detected in the experiment. Note that vortex shedding has also been shown to be inconsistent with instabilities observed in underwater systems [29].
- *Pendulum oscillations.* When it is aligned with the main stream, a pendulum motion of the sphere can be expected to appear with a characteristic frequency $f_p^{pend} = 1/2\pi\sqrt{T_{tip}/m_p L}$, where $T_{tip} = \pi/8 d^2 C_p U^2$ is the aerodynamic drag exerted on the sphere and $m_p \simeq 1.8$ mg is the mass of the sphere. In the range of particle Reynolds number considered here, the drag coefficient C_p is almost constant and of the order of 0.7. Hence f_p^{pend} can be estimated to increase almost linearly from 2 Hz to about 4 Hz when the wind speed is increased from 5 to 15 m s^{-1}. Such a low-frequency peak is not visible in the spectra in figure 7(a). Besides, the frequency peak would be expected to be modified when the cable length is changed. The few experiments we carried out with the longer cable show that the spectral peak reported in the previous section is not affected by the length of the cable.
- *Vibrating string frequencies.* One may also expect frequencies resulting from vibration modes of the tensed cable to appear. In the present case, where the cable has one fixed end and one free end, vibrating modes would have wavelengths $\lambda_n = 4L/(2n+1)$ (with $n \geqslant 0$). The corresponding eigenfrequencies are $f_p^n = (2n+1)/4L\sqrt{T_{tip}/\mu}$, where $\mu = 1.7$ mg m is the lineal density of the cable and T_{tip} is the main tensioning force due to aerodynamic drag on the sphere. We note that the given expression for f_p^n assumes the tension to be

constant along the cable and of the order of T_{tip}. This is not exactly the case, as frictional drag imposes a linear increase of the tension from the fixed upstream end of the cable to the downstream end (where tension is maximal and equal to T_{tip}). Hence, the estimation given here should be taken as an upper bound of the eigenfrequencies. Let us consider the case $U = 10\,\mathrm{m\,s^{-1}}$ as an example for discussion. Using $C_{\mathrm{p}} \simeq 0.7$, we estimate that $T_{\mathrm{tip}}^{10\mathrm{m\,s^{-1}}} \simeq 1.3 \times 10^{-3}\,\mathrm{N}$. The first ten vibrating eigenfrequencies are therefore expected to be $f_{\mathrm{p}}^{n=0\to 9}$[0.11; 0.32; 0.53; 0.74; 0.94; 1.2; 1.5; 1.6; 1.8; 2.0] Hz, and are much lower than the resonant peak observed in figure 7(a). Figure 9(b) shows that the experimental resonant peak for $U = 10\,\mathrm{m\,s^{-1}}$ appears at a frequency $f_{\mathrm{pk}} \gtrsim 20\,\mathrm{Hz}$. In the vibrating string scenario, this would correspond to a high-order mode ($f_{\mathrm{p}}^{100} \simeq 21\,\mathrm{Hz}$). Besides, in such a scenario, a whole set of eigenfrequencies should be visible in the spectra, which is not the case here. Finally, in this scenario, a length dependence would also be expected.

- *Elastic oscillation of the cable.* Another simple possible oscillatory mechanism would result from the elasticity of the cable. This would generate a natural oscillating frequency $f_{\mathrm{p}}^{\mathrm{elast}} = 1/2\pi\sqrt{k/m_{\mathrm{p}}}$, where k is the elastic constant of the cable. The constant k can be estimated from the elastic properties of nylon 6,6 given in table 1; it is of the order of $k = 2.3\,\mathrm{N\,m^{-1}}$. The elastic frequency is therefore expected to be of the order of 5 Hz. It is again much lower than the observed resonant peak. Besides, the elastic frequency is expected to remain independent of wind velocity, while figure 9(a) shows a clear increase of the resonant frequency f_{pk} as U increases. However, the order of magnitude of the elastic frequency may be consistent with the low-frequency plateau observed in figure 7(a) and this seems to be independent of U.

As a consequence, none of these simple mechanisms can explain the observed spectral peak. Our interpretation is that these oscillations are related to a *flutter* instability of the cable tip. This is also supported by the visual inspection that only a short section, a few centimeters long, in the vicinity of the downstream end of the cable is unstable. At first sight, *flutter* may appear contradictory to the qualitative conclusions of de Langre and Païdoussis concerning the requirement of a very well streamlined tip. However, the results of de Langre and Païdoussis cannot be directly extrapolated to the present case as the characteristic physical parameters differ by orders of magnitude. The base drag coefficient C_{b}, estimated from the aerodynamic drag on the sphere as $C_{\mathrm{b}} = \pi/4(d_{\mathrm{p}}/D)^2 C_{\mathrm{p}}$, exceeds for instance 10^4 in the experiment, while it is of order of at most 1 in simulations of de Langre and Païdoussis. We also note that in our experiment no *divergence* is observed prior to the oscillatory instability of the towed sphere.

4. Conclusion

We have reported our experimental investigation of the equilibrium and stability of a cable hanging in a uniform flow of air with one fixed end and three configurations for the free extremity: a free cable, a light polystyrene sphere and a heavy lead sphere. The system mimics the situation of a long towed cable at constant velocity in a steady environment. An important aspect of this work is the length-to-diameter ratio considered for the cable, which to our knowledge is the highest ever reported in experimental studies.

The average equilibrium position of the system is found to be consistently described by equations for the local average tension and angle of the cable given by Dowling [1] and estimates of drag coefficients for cables [25] and spheres [24] in the literature.

The stability analysis turned out to be an interesting fluid–structure coupling problem. Depending on the situation, we observed that the system could remain always stable (heavy towed particle) or could become unstable with either a *divergence* instability (when the cable is towed alone) or an oscillatory motion (when a light sphere is towed).

For the heavy particle, only small oscillations consistent with a pendular motion are observed. We note, however, that we could not reach velocities high enough for the cable to even approach an axial flow condition and the question of a possible instability at higher velocities is not excluded.

The case of the cable alone is found be qualitatively consistent with recent simulations of long cylinders in axial flows by de Langre and Païdoussis [16]. The threshold of the instability is found to coincide with the appearance of a neutral point at the downstream end of the cable. No secondary instability toward *flutter* was observed.

The instability for the light sphere exhibits oscillations with a clear resonant frequency which is inconsistent with simple mechanisms such as vortex shedding, pendular motion, string vibrations or elastic oscillations. We therefore interpret it as a *flutter* instability. This should be confirmed by further simulations of the cable stability, accounting for the particular boundary conditions associated with the presence of the sphere at the downstream tip.

From a practical point of view, our results may also be relevant for strategies of stabilization of towed systems, such as the use of weight depressors. Our experiment shows indeed that depending on the size and/or density of the added weight, the system can be stabilized or, in contrast, oscillations can be promoted.

Although much remains to be done to obtain a complete and reliable description of such long towed systems, we hope that this work will offer valuable experimental data to be confronted with future theoretical and numerical models. Experiments have also been carried out at present in turbulent conditions in order to explore the possible impact of turbulence on the reported instabilities and, more generally, on the dynamics of the towed object.

Acknowledgment

We thank Christophe Baudet, Yves Gagne and Nicolas Mordant for fruitful discussions.

References

[1] Dowling A P 1988 The dynamics of towed flexible cylinders: 1 and 2 *J. Fluid Mech.* **187** 507–71
[2] Jun Y W, Hall K R, Bennett A G and Bridges P D 1984 Optimal guidance for airborne cable pickup system *Proc. Guidance and Control Conf.* (*Seattle, WA*) pp 379–84
[3] Sgarioto D, Williams P and Trivailo P M 2006 Remote payload transportation using an aircraft-towed flexible cable system *ANZIAM J.* **47** 231–44
[4] Williams P, Sgarioto D and Trivailo P M 2008 Constrained path-planning for an aerial-towed cable system *Aerospace Sci. Technol.* **12** 347–54
[5] Quisenberry J E and Arena A S 2004 Dynamic simulation of low altitude aerial tow system *AIAA Atmospheric Flight Mechanics Conf. and Exhibit* (*Providence, RI*) p 4813
[6] Siebert H, Gerashchenko S, Gylfason A, Lehmann K, Collins L R, Shaw R A and Warhaft Z 2010 Towards understanding the role of turbulence on droplets in clouds: *in situ* and laboratory measurements *Atmos. Res.* **97** 426–37
[7] Choo Y I and Casarella M J 1973 A survey of analytical methods for dynamic simulation of cable-body systems *J. Hydronaut.* **7** 137–44

[8] Kamman J W, Nguyen T C and Crane J W 1990 Modeling towed cable systems dynamics *Technical Report* (Panama City, FL: Naval Coastal Systems Center)
[9] Sudarsan K, Bhattacharyya S K and Vendhan C P 1997 An experimental study of hydroelastic instability of flexible towed underwater cylindrical structures *Proc. 16th Offshore Mechanics and Arctic Engineering Conf. (OMAE '97) (Yokohama, Japan, 13–18 April 1997)* pp 73–80
[10] Theodoracatos V E and Calkins D E 1986 An experimental study of elastohydrodynamics of towed flexible cylinders aided by video image processing *Ocean Eng.* **13** 587–619
[11] Paidoussis M P 1966 Dynamics of flexible slender cylinders in axial flow: 1. Theory *J. Fluid Mech.* **26** 717–36
[12] Ortloff C R and Ives J 1969 On the dynamic motion of a thin flexible cylinder in a viscous stream *J. Fluid Mech.* **38** 713–20
[13] Païdoussis M P 1973 Dynamics of cylindrical structures subjected to axial flow *J. Sound Vib.* **29** 365–85
[14] Ni C C and Hansen R J 1978 An experimental study of the flow-induced motions of a flexible cylinder in axial flow *J. Fluids Eng.* **100** 389–95
[15] Schouveiler L, Eloy C and le Gal P 2005 Flow-induced vibrations of high mass ratio flexible filaments freely hanging in a flow *Phys. Fluids* **17** 047104
[16] de Langre E and Paidoussis M P 2007 Flutter of long flexible cylinders in axial flow *J. Fluid Mech.* **571** 371–89
[17] Bhattacharyya S K, Vendhan C P and Sudarsan K 2000 The finite element method for hydroelastic instability of underwater towed cylindrical structures *J. Sound Vib.* **237** 119–43
[18] Païdoussis M P, Grinevich E, Adamovic D and Semler C 2002 Linear and nonlinear dynamics of cantilevered cylinders in axial flow: 1. Physical dynamics *J. Fluids Struct.* **16** 691–713
[19] Semler C, Lopes J L, Augu N and Païdoussis M P 2002 Linear and nonlinear dynamics of cantilevered cylinders in axial flow: 3. Nonlinear dynamics *J. Fluids Struct.* **16** 739–59
[20] Paidoussis M P 2003 *Fluid–Structure Interactions: Slender Structures and Axial Flows* vol 2 (Amsterdam: Elsevier)
[21] Triantafyllou G S and Chryssostomidis C 1985 Stability of a string in axial flow *ASME J. Energy Resour. Technol.* **107** 421–5
[22] Hoerner S F 1965 *Fluid-Dynamic Drag: Practical Information on Aerodynamic Drag and Hydrodynamic Resistance* (Bricktown, NJ: Hoerner Fluid Dynamics)
[23] Pode L 1951 Tables for computing the equilibrium configuration of a flexible cable in a uniform stream *Technical Report No. DTMB-687* (Washington, DC: David Taylor Model Basin)
[24] Brown P P and Lawler D F 2003 Sphere drag and settling velocity revisited *J. Environ. Eng.* **129** 222–31
[25] Tritton D J 1959 Experiments on the flow past a circular cylinder at low Reynolds numbers *J. Fluid Mech.* **6** 547–67
[26] Taylor G 1952 Analysis of the swimming of long and narrow animals *Proc. R. Soc. Lond.* A **214** 158–83
[27] Wei C Y and Kukureka S N 2000 Evaluation of damping and elastic properties of composites and composite structures by the resonance technique *J. Mater. Sci.* **35** 3785–92
[28] Lalu P P 2011 Effect of bending rigidity of marine cables on the dynamic stability of two-part underwater towing system *Int. J. Eng. Sci. Technol.* **3** 5599–608
[29] Bandyopadhyay P R, Leinhos H A, Hrubes J D, Toplosky N and Hansen J 2011 Turning of a short-length cable using flapping fin propulsion *IEEE J. Ocean. Eng.* **36** 571–85